ISSN 1547-4771, Physics of Particles and Nuclei Letters, 2024, Vol. 21, No. 2, pp. 131–139. © Pleiades Publishing, Ltd., 2024.
Russian Text © The Author(s), 2024, published in Pis'ma v Zhurnal Fizika Elementarnykh Chastits i Atomnogo Yadra, 2024.

METHODS OF PHYSICAL EXPERIMENT

Characteristics of Coherent Transition Radiation in the Prewave Zone from a Finite-Size Target

A. P. Potylitsyn[a], A. A. Baldin[b, g], V. V. Bleko[f], A. V. Vukolov[a], G. A. Naumenko[a], P. V. Karataev[d], V. V. Kobets[b], V. R. Kocharyan[e], A. S. Kubankin[c], M. M. Toktaganova[a], M. V. Shevelev[a], D. A. Shkitov[a], V. V. Bleko[b, g, *], D. S. Korovkin[b], I. A. Kishin[c], and E. Yu. Kidanova[c]

[a] *Tomsk Polytechnic University, Tomsk, 634050 Russia*
[b] *Joint Institute for Nuclear Research, Dubna, 141980 Russia*
[c] *Belgorod State University, Belgorod, 308015 Russia*
[d] *John Adams Institute at Royal Holloway, University of London, United Kingdom*
[e] *Institute of Applied Problem of Physics of National Academy of Sciences of the Republic of Armenia, Yerevan, Republic of Armenia*
[f] *MIREA–Russian Technological University, Moscow, 119454 Russia*
[g] *Institute for Advanced Study "OMEGA", Dubna, 141896 Russia*
*****e-mail: vbleko@jinr.ru*

Received April 7, 2023; revised November 7, 2023; accepted November 7, 2023

Abstract—Results of experimental and theoretical investigation of coherent transition radiation from a finite-size target in the prewave zone are presented. The measurements were conducted in sub-terahertz frequency range on the 100-MeV electron beam extracted from LINAC-200 (JINR). A formula for the spectral-angular density of coherent transition radiation is obtained. Results of the simulation of experimental conditions and experimental data are jointly analyzed. Estimation of the bunch length based on experimental data and obtained theoretical model deviates from the expected value.

DOI: 10.1134/S1547477124020110

INTRODUCTION

The mechanism of coherent transition radiation (CTR) has been studied relatively well [1, 2] and is used, for example, for diagnosing short electron bunches [3, 4]. The same mechanism was employed in [5, 6] to form operational beams of electromagnetic radiation in the terahertz range at accelerators with electron energy $E_e > 100$ MeV. It should be noted that in [5, 6] the target parameters, the geometry of the CTR generation process, and the optics of CTR beam formation were not optimized. The angular distribution of CTR relative to the direction of specular reflection is "funnel-shaped" with a zero minimum along the axis. The angular distribution in the "far zone" is known not to depend on the wavelength and to be determined by the inverse Lorentz factor ($\theta_m \sim \gamma^{-1}$). In the so-called "prewave zone" [7, 8], the angular distribution of CTR is also "funnel-shaped", but the polar angle θ_m that correspond to the distribution maximum depends on the wavelength and target size, and, usually, $\theta_m \gg \gamma^{-1}$.

The standard definition of far field [9]

$$D \gg \ell_f = \gamma\lambda, \quad (1)$$

where ℓ_f is the radiation formation length is only valid if the characteristic size of the target (radius R_T) is much larger than the radius of the Coulomb field of the charge

$$R_T \gg \gamma\lambda. \quad (2)$$

If condition (2) is not fulfilled, the concept of "far zone", which determines the distance to the target at which the radiation source can be considered as a point (angle θ_m does not depend on the distance), alters, and relation (1) is no longer valid. In the THz range ($\lambda \leq 1$ mm) the TR process corresponds to the prewave zone, i.e., the angular "opening" of the CTR cone of relativistic electrons is determined by the distance D between the target and the detector and target radius R_T and depends on the wavelength λ.

EXPERIMENT

An experiment to study the CTR characteristics was carried out on the electron beam of the LINAC-200 accelerator [10, 11]. The main parameters of the electron beam are presented in Table 1.

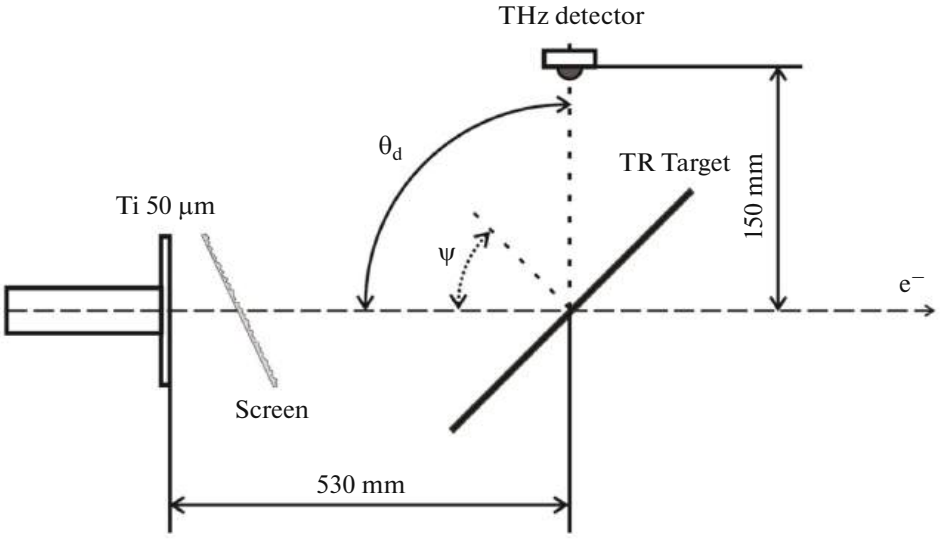

Fig. 1. Experimental setup.

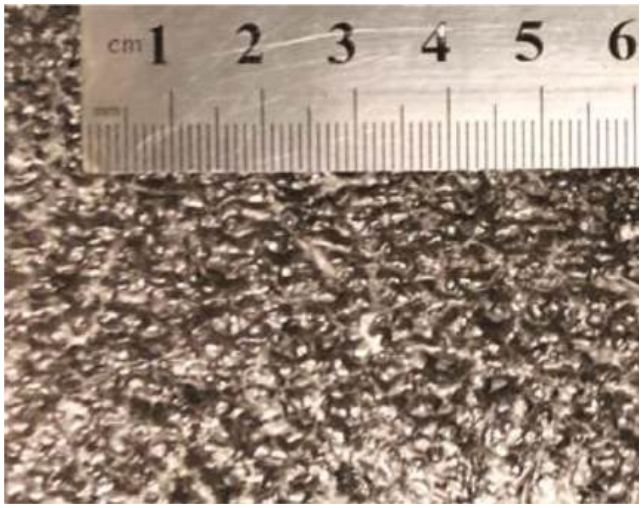

Fig. 2. Image of the scattering screen.

The measurements were carried out with the electron energy $E_e = 100$ MeV and current 16 mA. The experimental setup is displayed in Fig. 1.

The beam exited through a titanium foil 50 μm thick and passed through a scattering screen made of foamed polyethylene with a total thickness of 0.028 g/cm^2, whose metallized side faced the nozzle (of aluminum coating thickness 10 μm), and impinge on the transition radiation target (foiled textolite, metal coating thickness 18 μm). The image of the scattering screen is displayed in Fig. 2. A target (size 150×100 mm) was placed in a goniometer, so that it can be rotated around a vertical axis coinciding with the electron beam with an accuracy of 0.1°. At a fixed angle $\theta_d = 90°$ relative to the electron beam, the detector (Schottky diode, see Fig. 3) was located at a distance of 150 mm. Detector sensitivity rating band [12] is 100—700 GHz with sensitivity 10 V/W.

Table 1. Characteristics of the LINAC-200 accelerator

Electron energy E_e	26–200 MeV
Macropulse duration	30–3000 ns
Micropulse length	$\sigma_z = 0.3$ mm
Accelerated current	0–60 mA
HF frequency	2865 MHz

The scattering screen "separated" the transition radiation from the exit titanium window. Measurements of the transition radiation yield in the visible range directly from the screen showed that its intensity is below the sensitivity threshold of the equipment we used. The duration of dumping electrons onto the target was 2 μs at a dumping frequency of 10 Hz.

The accelerated current was measured using an induction sensor, the signal from which was analyzed concurrently with the signal from the detector. At each point where the orientation dependence of the CTR yield was measured, information was collected in 3 macropulses.

Figure 4 shows the dependence of the CTR yield measured by the detector on the target orientation angle ψ. As expected, when the condition $\theta_d = 2\psi$ is fulfilled (i.e., when $\psi = 45°$), a minimum radiation intensity is observed. It should be noted that the position of the maximum in the measured orientation dependence $\psi_m = 3.55 \pm 0.4°$ corresponds to the angle $\theta_m = 2\psi_m = 7.1°$ in the angular distribution of transition radiation [13]. It is apparent that the formation of an aperture whose axis coincides with that of the CTR cone, where the radiation intensity is minimal, as it was done in [5], is not optimal.

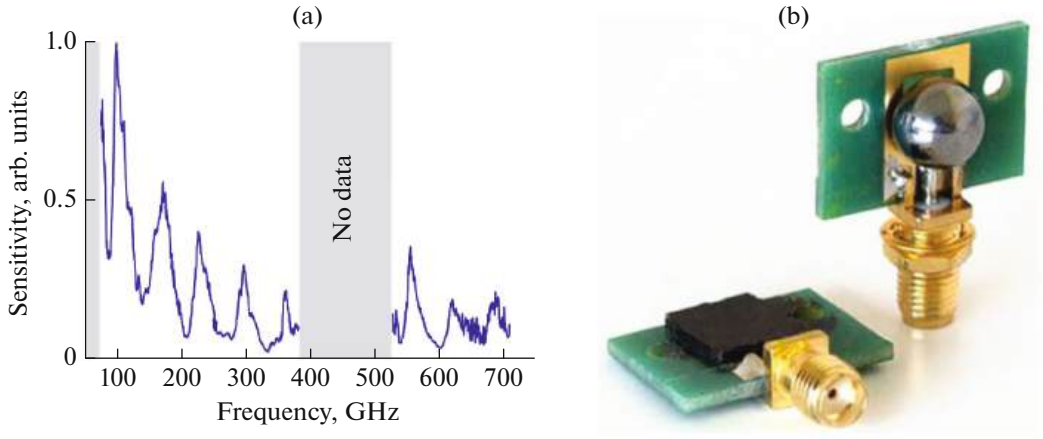

Fig. 3. Detector based on Schottky diode. (a) Spectral range of sensitivity; (b) image of the detector [12], entry lens diameter (aperture) is 9 mm.

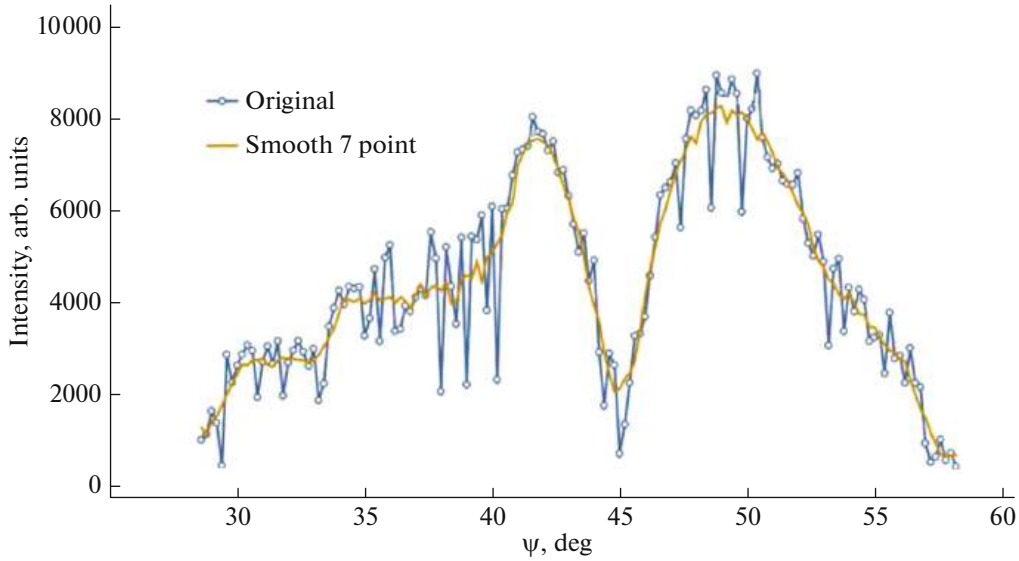

Fig. 4. CTR intensity measured with the detector oriented at an angle $\theta_d = 90°$ relative to the electron beam as a function the target rotation angle.

Figure 5 displays the measured dependence of the detector output signal Y on the accelerated current I, which is approximated by the formula

$$Y = 1.75 + 0.31 \times I^{1.59}. \quad (3)$$

Full coherence corresponding to the exponent $n = 2$ in our case was not achieved, most likely due to the significant transverse size of the electron beam ($d \sim 4.5$ mm $\gg \sigma_z$), see, for example, [14, 15]. Another possible reason is that the detector band does not fully "span" the radiation coherence region.

MODEL

The CTR spectrum is primarily determined by the so-called "longitudinal form factor"

$$F_L = \left| \int dz S_L(z) \exp(-i\omega z/c) \right|^2, \quad (4)$$

where $S_L(z)$ is the distribution of electrons in a bunch along the propagation velocity. This distribution is usually well described by a Gaussian with the parameter σ_z. In this case, from Eq. (4) we obtain

$$F_L(\omega) = \exp\left[-\omega^2 \sigma_z^2\right]. \quad (5)$$

Spectral distribution of the CTR bunch with population N_e is represented as [14]:

$$\frac{d^2W_{CTR}}{d\omega d\Omega} = \frac{d^2W_{TR}}{d\omega d\Omega}\left[N_e + N_e(N_e - 1)\right] F_L(\omega), \quad (6)$$

where $\frac{d^2W_{TR}}{d\omega\, d\Omega}$ is the spectral-angular distribution of a single-electron TR (incoherent TR). In the approxi-

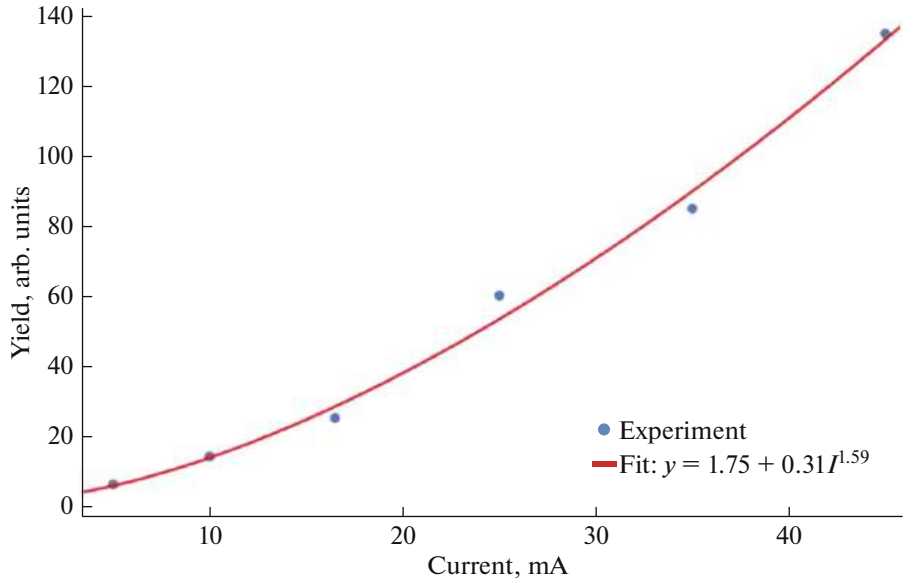

Fig. 5. Dependence of the signal from the detector on the accelerated current.

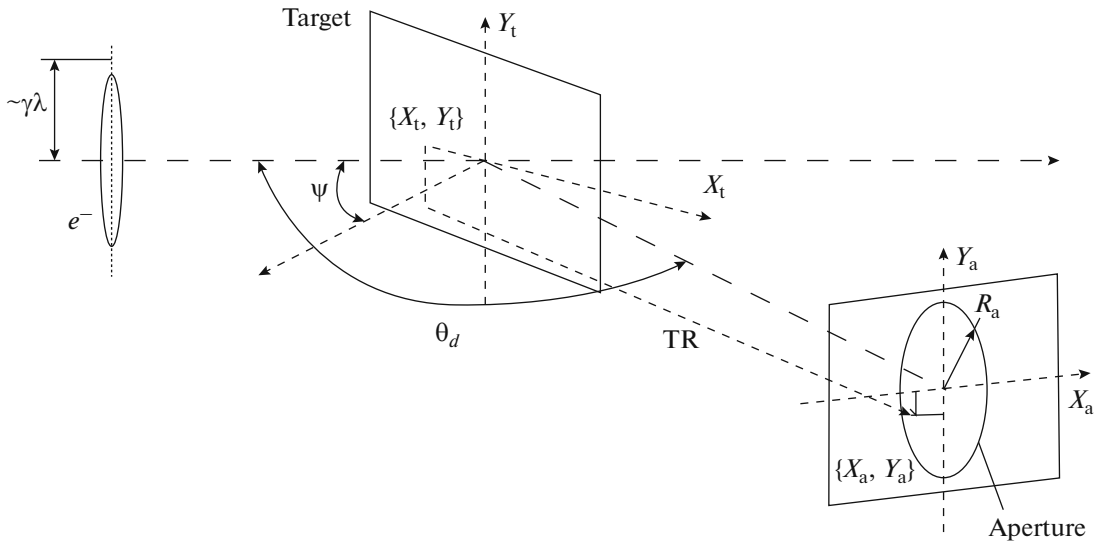

Fig. 6. Scheme of the formation of a CTR beam with an aperture diameter $2R_a$ located at a distance D from the center of the target T.

mation used below, the contribution of the transverse form factor along with the difference between the actual optical characteristics of the target and an ideal conductor are neglected. In this approximation, the characteristics of the "backward" (BTR) and "forward" (FTR) transition radiation coincide [15] provided that the angular characteristics of the BTR are expressed in terms of angles measured from the specular reflection direction.

We calculate the characteristics of incoherent TR using the model [8], based on the pseudophoton model. The TR field generated by a relativistic electron in a target of finite dimensions $2x_m \times 2y_m$ (see the diagram in Fig. 6) after integration over area S_T is represented as:

$$\begin{Bmatrix} E_x(\theta_x,\theta_y) \\ E_y(\theta_x,\theta_y) \end{Bmatrix} = A_1 \int_{ST} d\sigma \begin{Bmatrix} x_T \\ y_T \end{Bmatrix} \frac{K_1\left(k\sqrt{x_T^2+y_T^2}\right)}{\sqrt{x_T^2+y_T^2}} \times \exp\left\{ i\pi \left[\frac{x_T^2+y_T^2}{D\lambda} - 2\frac{x_T\gamma\theta_x + y_T\gamma\theta_x}{\lambda} \right] \right\} = A_1 \begin{Bmatrix} I_x^{TR}(\theta_x,\theta_y) \\ I_y^{TR}(\theta_x,\theta_y) \end{Bmatrix}. \quad (7)$$

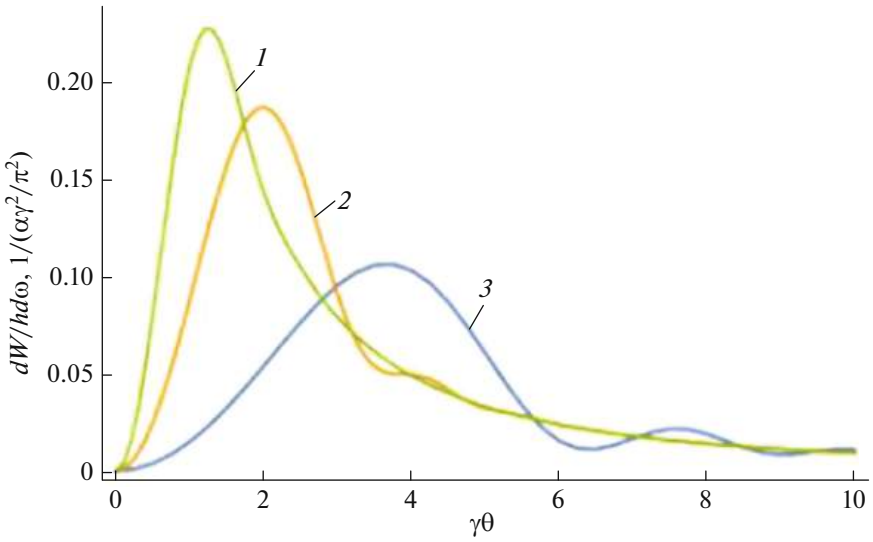

Fig. 7. Angular distributions of transition radiation with a fixed wavelength $\lambda = 0.3$ mm at various distances from the target in the pre-wave zone for $\gamma = 100$: green curve (*1*) $D = 1500$ mm; yellow curve (*2*) $D = 500$ mm; blue curve (*3*) $D = 150$ mm.

Here S_T is the target area, $d\sigma = dx_T\, dy_T$, x_T, y_T are coordinates on the target surface ($-x_m < x_T < x_m$, $-y_m < y_T < y_m$), $\theta_x = x_a/D$, $\theta_y = y_a/D$ (x_a, y_a are coordinates on the aperture plane located at a distance D away from the target), $k = 2\pi/\lambda$, λ is the wavelength, and $K_1(x)$ is the Bessel function.

The resulting expression for the spectral-angular distribution of the TR in the case under consideration has the form $\left(A_1^2 = e^2\gamma^2/\pi^2c^2\, 1/8\pi\sqrt{2}\right)$:

$$\frac{d^2W_{TR}}{d\omega d\Omega} = c\left(\left|E_x(\theta_x,\theta_y)\right|^2 + \left|E_y(\theta_x,\theta_y)\right|^2\right) = \frac{e^2\gamma^2}{\pi^2 c}\frac{1}{8\pi\sqrt{2}}\left(\left|I_x^{TR}(\theta_x,\theta_y)\right|^2 + \left|I_y^{TR}(\theta_x,\theta_y)\right|^2\right). \quad (8)$$

To illustrate the dependence of the angular distribution of incoherent TR from the finite-size target on the distance D between the target and the aperture, we consider a target in the form of a disk with a cone R_T. In passing to polar coordinates, Eq. (7) is replaced with:

$$\frac{d^2W_{TR}}{d\omega d\Omega} = c\,A_2^2\left|\int_0^{R_T} K_1(k\,r_T)\exp\left\{i\pi\left[\frac{r_T^2}{D\lambda} - 2\frac{r_T r_a}{D\lambda}\cos(\varphi_T - \varphi_a)\right]\right\} r_T dr_T\, d\varphi_T\right|^2, \quad (9)$$

where $r_a = D\sin\theta \approx D\theta$, $c\,A_2^2 = e^2\gamma^2/\pi^2 c$.

Figure 7 shows the "broadening" of the angular distribution of TR as the distance D decreases. For example, for the distance $D = 150$ mm, the angular distribution of TR reaches a maximum at $\gamma\theta_{max} = 4$ for $\gamma = 100$, $\lambda = 0.3$ mm, and $R_T = 50$ mm.

As the TR wavelength increases, a further "broadening" of the distribution is observed (see Fig. 8). As follows from the results obtained, by measuring the angular distribution of CTR, it is possible to estimate the "average" wavelength of the detected spectral range based on the value of θ_{max}. Indeed, this value does not depend on the longitudinal form factor.

As shown in [13, 15], the same information can be obtained from measurements of the orientation dependence of the TR yield at a fixed detector position $\theta_d = \text{const}$. The orientation dependence is calculated using the same formulas (8) with replacements

$$\theta_x = 2\Delta\psi,\ \Delta\psi = \psi - \theta_d/2. \quad (10)$$

Substitution (10) corresponds to the "reflection" of the TR beam from the target as it rotates around the vertical axis.

Figure 9 shows typical orientation dependences of TR from a target with dimensions $2x_m \times 2y_m = 150 \times 100$ mm at the distance $D = 150$ mm. Zero value of angle ψ corresponds to a target rotation angle of 45°. As follows from the figure, for the wavelength $\lambda = 3$ mm

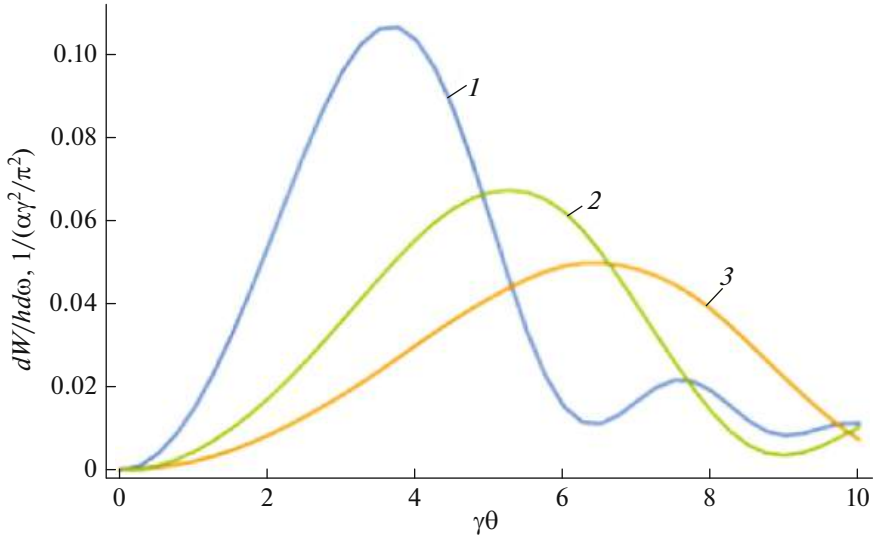

Fig. 8. Angular distributions of transition radiation with various wavelengths for a fixed distance between the target and the aperture $D = 150$ mm at $\gamma = 100$: blue curve (*1*) $\lambda = 0.3$ mm; green curve (*2*) $\lambda = 0.6$ mm; yellow curve (*3*) $\lambda = 0.9$ mm.

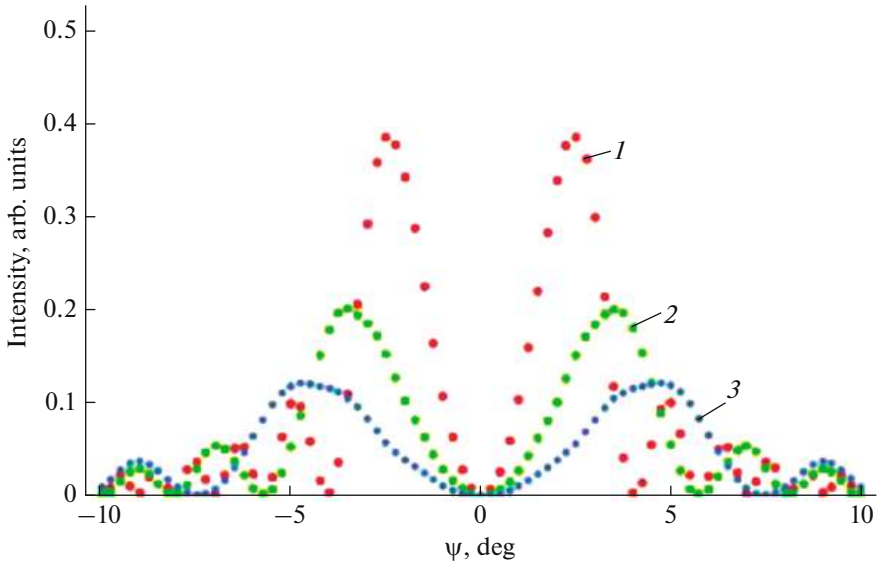

Fig. 9. Dependence of TR intensity on the target rotation angle for $\gamma = 100$ and $D = 150$ mm at fixed observation angle $\theta_d = 90°$ for various wavelengths: red curve (*1*) $\lambda = 1.5$ mm; green curve (*2*) $\lambda = 3$ mm; blue curve (*3*) $\lambda = 5$ mm.

($\nu = 100$ GHz), the angular distance between the maxima is 7.2°, which is close to the experimental value, while similar values for $\lambda = 1.5$ mm and $\lambda = 5$ mm do not coincide with experiment. It should be noted that the displayed dependences were obtained for a point detector located at point {0, 0} (see Fig. 6).

If the CTR beam is formed using a finite aperture (which in our case is the aperture of the detector input lens with a diameter of 9 mm, or, as in experiment [5], the output window of the vacuum chamber), it is necessary to integrate Eqs. (8) and (9) over the aperture (taking into account the form factor) to obtain the CTR beam spectrum. If the aperture is oriented at an angle θ_d, due to azimuthal symmetry, the desired result is reduced to a single integral

$$\frac{d^2W_{TR}}{d\omega d\Omega} \to \frac{dW_{TR}}{d\omega} = 2\pi \int_0^{\theta_{max}} \theta d\theta \frac{d^2W_{TR}}{d\omega d\Omega}, \qquad (11)$$

where $\theta_{max} = R_a/D$ and, consequently,

$$\frac{dW_{CTR}}{d\omega} = \frac{dW_{TR}}{d\omega} F_L(\omega). \qquad (12)$$

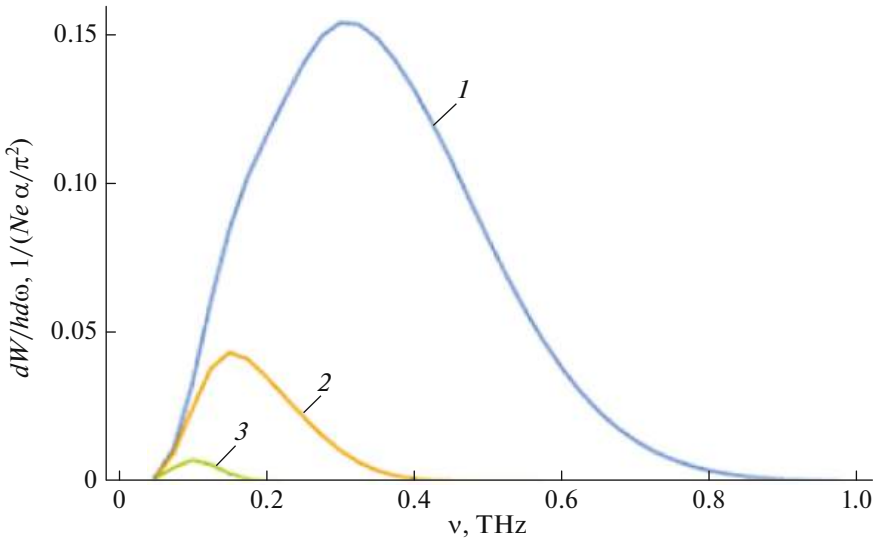

Fig. 10. CTR spectra for aperture $R_a = 4.5$ mm oriented at an angle $\theta_d = 2\psi$ ($\psi = 45°$) at $\gamma = 200$ and $D = 150$ mm: blue curve (*1*) bunch length $\sigma_z = 0.15$ mm; yellow curve (*2*) $\sigma_z = 0.3$ mm; green curve (*3*) $\sigma_z = 0.6$ mm.

If the beam is formed by an aperture located close to the angle θ_{max}, corresponding to the maximum radiation intensity (see Fig. 8) or, in other words, if the target is oriented at an angle $\psi = \frac{\theta_d}{2} + \frac{\theta_{max}}{2}$ (see Fig. 9), azimuthal symmetry is violated, and double integration of Eq. (8) over angles θ_x, θ_y is required provided the condition $\theta_x^2 + \theta_y^2 \le (R_a/D)^2$ is fulfilled.

Figure 10 displays the CTR spectra for the case $\psi = \theta_d/2$, i.e., when aperture $R_a = 4.5$ mm is located symmetrically relative to the specular reflection direction at the distance $D = 150$ mm. As follows from the figure, the CTR spectrum for a bunch with $\sigma_z = 0.3$ mm is concentrated near the frequency of 160 GHz, i.e., in the range where the detector sensitivity reaches 50% of the maximum value (see Fig. 3). Figure 11 presents similar spectra for the same aperture, but with the target rotated by an angle $\Delta\psi = 3.5°$, i.e., the configuration in which the aperture location corresponds to the maximum CTR yield. In this case, the maximum in the CTR beam spectrum for $\sigma_z = 0.3$ mm lies in the region of 100 GHz, but the intensity is significantly higher.

The same figure shows the spectrum of incoherent TR (blue) for the same conditions.

RESULTS, DISCUSSION, AND CONCLUSIONS

As mentioned above, for beams of relativistic electrons ($\gamma \gg 100$) the geometric size of the target for TR generation is usually significantly smaller than the transverse size of the Coulomb field at $\lambda \sim 1$ mm. For such a geometry, the angular distribution of TR is determined by the quantities R_T, D, and λ and does not depend on the Lorentz factor. Therefore, to form a radiation beam in the THz/sub-THz range using the CTR mechanism, it is necessary to optimize both the indicated parameters and the geometry of the aperture location (see Figs. 10 and 11). Choosing the relationship between target size and magnitude $\gamma\lambda$, it is possible to adjust the "cutoff" of the CTR spectrum in the "soft" part. In the "hard" part of the spectrum, the "cutoff" is determined by the form factor, which leads to the emergence of an effective spectral "band" (see Fig. 11). By measuring the orientation dependence of the CTR yield, the central frequency of this band can be identified.

Based on the CTR spectra calculated per electron (see Fig. 11), it is possible to estimate the energy emitted by one bunch consisting of N_e electrons and, therefore, the energy of all bunches in the macropulse N_b:

$$\Delta W_B = N_b (N_e)^2 \frac{\alpha}{\pi^2} 2\pi\hbar \int_{\nu_{min}}^{\nu_{max}} \frac{dW_{CTR}}{\hbar\, d\omega} d\nu. \qquad (13)$$

In Eq. (13), $\frac{dW_{CTR}}{\hbar\, d\omega}$ are the spectra displayed in Fig. 11 and ν_{min}, ν_{max} are the detector sensitivity band ($\nu_{min} = 100$ GHz, $\nu_{max} = 700$ GHz). We carried out measurements at an accelerated current of 16 mA, which, for a macropulse duration of 2 μs and an RF field frequency of 2865 MHz, corresponds to the following parameters: $N_e = 0.37 \times 10^8$ and $N_b = 5.4 \times 10^3$. Estimated energy emitted by one bunch and the radiation

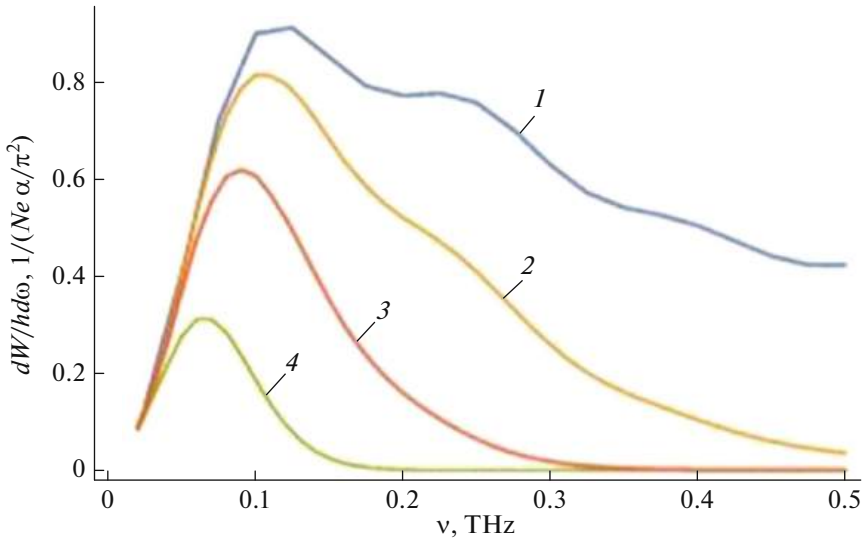

Fig. 11. The same for the target rotation angle $\psi = 48.5°$: blue curve (*1*) spectrum of incoherent transition radiation; yellow curve (*2*) bunch length $\sigma_z = 0.15$ mm; orange curve (*3*) $\sigma_z = 0.3$ mm; green curve (*4*) $\sigma_z = 0.6$ mm.

power per macropulse (number of bunches $N_b = 5.4\times10^3$) are presented in Table 2.

The certified efficiency of our detector is ~10 V/W, and the signal level measured in the experiment is ~20 mV, which corresponds to a power level of ~2 mW. A comparison with the estimates in Table 2 shows that the duration of the LINAC-200 accelerator bunch exceeds the expected value ($\sigma_z > 0.3$ mm).

The correctness of the model was tested in estimating the CTR beam energy reported in [5] (see Fig. 13) $\Delta W_B \sim 25\times10^{-6}$ J. An estimation based on the model used for the experimental parameters [5] ($\sigma_z = 15$ fs, $Q = 0.1$ nC, $\gamma = 1000$, $R_T = 12.5$ mm, $D = 40$ mm, $R_a = 10$ mm) yields $\Delta W_B \sim 40\times10^{-6}$ J, a value which is fairly close to the experiment.

Summarizing, we note that the existing parameters of the LINAC-200 accelerator enable conducting calibration measurements of equipment in the sub-THz range.

Table 2. Energy emitted by an electron bunch per micropulse and the radiation power during a 2-μs-long macropulse

σ_z, mm	ΔW_B, eV	P, W
0.15	5.6×10^8	240×10^{-3}
0.30	1.8×10^8	80×10^{-3}
0.60	2.4×10^7	10×10^{-3}

FUNDING

This work was supported by the Ministry of Education and Science of the Russian Federation (program "Science" no. FSWW-2023-0003).

CONFLICT OF INTEREST

The authors of this work declare that they have no conflicts of interest.

REFERENCES

1. M. Castellano, A. Cianchi, G. Orlandi, and V. A. Verzilov, "Effects of diffraction and target finite size on coherent transition radiation spectra in bunch length measurements," Nucl. Instrum. Methods Phys. Res., Sect. A **435**, 297 (1999).
2. C. B. Schroeder, E. Esarey, J. van Tilborg, and W. P. Leemans, "Theory of coherent transition radiation generated at a plasma-vacuum interface," Phys. Rev. E **69**, 016501 (2004).
3. S. Wesch, B. Schmidt, C. Behrens, H. Delsim-Hashemi, and P. Schmuser, Nucl. Instrum. Methods Phys. Res., Sect. A **665**, 40 (2011).
4. I. Nozawa, K. Kan, J. Yang, et al., "Measurement of <20 fs bunch length using coherent transition radiation," Phys. Rev. Spec. Top.–Accel. Beams **17**, 072803 (2014).
5. S. Casalbuoni, B. Schmidt, and P. Schmuser, V. Arsov, and S. Wesch, "Ultrabroadband terahertz source and beamline based on coherent transition radiation," Phys. Rev. Spec. Top.–Accel. Beams **12**, 030705 (2009).
6. E. Chiadroni, M. P. Anania, M. Artioli, et al., "Two color FEL driven by a comb-like electron beam distribution," Rev. Sci. Instrum. **84**, 022703 (2013).

7. V. Verzilov, "Transition radiation in the pre-wave zone," Phys. Lett. A **273**, 135 (2000).
8. A. P. Potylitsyn, "Image of Optical Diffraction Radiation (ODR) Source and Spatial Resolution of ODR Beam Profile Monitor," in *Advanced Radiation Sources and Applications, NATO Science Series II: Mathematics, Physics and Chemistry* (Springer, 2006), Vol. 199, p. 149.
9. X. Artru, R. Chehab, K. Honkavaara, and A. Variola, "Resolution power of optical transition radiation: theoretical considerations," Nucl. Instrum. Methods Phys. Res., Sect. B **145**, 160 (1998).
10. A. A. Baldin et al., "FLAP collaboration," Phys. Elem. Part. At. Nucl. **18**, 281 (2021).
11. N. I. Balalykin et al., "Status of the LINAC-800 construction at JINR," in *Proceedings of LINAC08, Victoria, BC, Canada, 2008*, pp. 480–482.
12. https://terasense.com/products/detectors/.
13. A. N. Aleinik, O. V. Chefonov, B. N. Kalinin, et al., "Low-energy electron-beam diagnostics based on the optical transition radiation," Nucl. Instrum. Methods Phys. Res., Sect. A **201**, 34 (2003).
14. Y. Shibata, K. Ishi, T. Takahashi, et al., "Coherent transition radiation in the far-infrared region," Phys. Rev. E **49**, 785 (1994).
15. A. P. Potylitsyn, "Transition radiation and diffraction radiation. similarities and differences," Nucl. Instrum. Methods Phys. Res., Sect. B **145**, 169 (1998).